ACS OMEGA

Article

http://pubs.acs.org/journal/acsodf

Co_3O_4 Nanowires on Flexible Carbon Fabric as a Binder-Free Electrode for All Solid-State Symmetric Supercapacitor

Promita Howli,[†,§] Swati Das,[†] Samrat Sarkar,[‡] Madhupriya Samanta,[‡] Karamjyoti Panigrahi,[‡] Nirmalya Sankar Das,[‡,∥] and Kalyan Kumar Chattopadhyay*[,†,‡]

[†]Department of Physics and [‡]School of Materials Science and Nanotechnology, Jadavpur University, Kolkata 700032, India

W *Web-Enhanced Feature* *S* *Supporting Information*

ABSTRACT: Developing portable, lightweight, and flexible energy storage systems has become a necessity with the advent of wearable electronic devices in our modern society. This work focuses on the fabrication of Co_3O_4 nanowires on a flexible carbon fabric (CoNW/CF) substrate by a simple cost-effective hydrothermal route. The merits of the high surface area of the prepared Co_3O_4 nanostructures result in an exceptionally high specific capacitance of 3290 F/g at a scan rate of 5 mV/s, which is close to their theoretical specific capacitance. Furthermore, a solid-state symmetric supercapacitor (SSC) based on CoNW/CF (CoNW/CF//CoNW/CF) was fabricated successfully. The device attains high energy and power densities of 6.7 Wh/kg and 5000 W/kg. It also demonstrates excellent rate capability and retains 95.3% of its initial capacitance after 5000 cycles. Further, the SSC holds its excellent performance at severe bending conditions. When a series assembly of four such devices is charged, it can store sufficient energy to power a series combination of five light-emitting diodes. Thus, this SSC device based on a three-dimensional coaxial architecture opens up new strategies for the design of next-generation flexible supercapacitors.

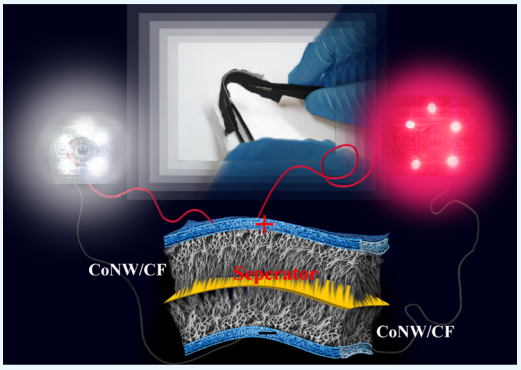

INTRODUCTION

Modern civilization is surrounded by myriads of gadgets, chiefly based on sensors and communication devices. With gradual miniaturization, these gadgets have become wearable, leading to the necessity of being flexible and portable. Parallel research has been culminating in the development of energy storage devices to power these gadgets that should themselves be flexible and lightweight. Supercapacitors and lithium ion batteries are two major electrochemical energy storage devices.[1−4] They have a lot of advantages, such as their low cost, long life span, and good reversibility, and most importantly, they are environment benign. Owing to their high power density, supercapacitors are hugely popular as power sources in portable electronic devices such as mobile phones, e-readers, laptops, etc.[5−9] It is well established that supercapacitors are a bridge between the conventional battery and dielectric capacitor. However, their main shortcoming is their low energy density due to their low working potential in comparison to batteries.[10] So, it is a big challenge among the research community to fabricate such materials with improved energy density to meet the higher requirements necessary for future technologies. Supercapacitors can be categorized into two types on the basis of their charge storage mechanism: electric double layer capacitors (EDLCs) and pseudocapacitors. EDLCs store electrical energy by electrostatic accumulation of charges on the electrode−electrolyte interface, whereas in the case of pseudocapacitors, fast and reversible redox reactions occur on the surface of the electrode, exhibiting much higher specific capacitance than EDLCs.[11] To date, carbonaceous materials (activated carbon, graphene oxide, carbon nanotubes, etc.)[12−17] have been used as supercapacitor electrode materials due to their good cyclic stability, however, they have not excelled because of their low specific capacitance, which diminished the energy density of the fabricated supercapacitors. To meet ever-increasing energy demands, various inorganic metal oxides/hydroxides, such as MnO_2, RuO_2, CuO, NiO, V_2O_5, WO_3, $Co(OH)_2$, $Ni(OH)_2$, etc.,[18−28] have been used as electrode materials in electrochemical energy storage. Also, conducting polymers, such as polyaniline, polypyrrole, etc., are frequently used with metal oxides to improve their electrochemical performance.[29−31] Among researchers nowadays, it is a great challenge to improve capacitive behavior.

It is now well known that nanostructures of different metal oxides have several advantages in various fields of potential applications as well as in supercapacitors. However, low electrical conductivity limits the performance of the metal oxide nanostructures as pseudocapacitor materials. Additionally, in the conventional procedure of electrode preparation, additives block a large part of the electroactive materials from contacting with the electrolyte properly, so only the surface part of the materials are utilized and effectively contribute to the total capacitance. Henceforth, an improved design of electrode

Received: May 30, 2017
Accepted: July 13, 2017
Published: August 3, 2017

DOI: 10.1021/acsomega.7b00702
ACS Omega 2017, 2, 4216−4226

architecture is hugely needed to boost specific capacitance as well as the electrochemical usability of these pseudocapacitor materials. In this regard, recently, metal oxide nanostructures have been directly grown on various conductive substrates such as poly(ethylene terephthalate), copper foil, Ni foam, etc.[21,32,33] By using this technique, many competitive advantages can be acquired, such as a high amount of electron accessibility, fast ion transportation, and easy diffusion of the electrolyte. Carbon fabric (CF) is one of the most ideal substrates for the growth of nanostructures because of its superior electrical conductivity and good mechanical stability. In flexible power devices for modern electronic gadgets, lightweight as well as bendable current collectors are used, and for this purpose, CF is the most worthy candidate as a flexible current collector. There are several reports regarding supercapacitors composed of a metal oxide grown on a CF substrate.[34−37] Cobalt oxide has been used a great deal in the supercapacitor field as a promising pseudocapacitor material. There are many reports on the use of different morphologies of Co_3O_4 to enhance capacitive behavior. For example, Yang et al. reported ultrathin Co_3O_4 nanosheets,[38] Shim et al. reported flower-like microspheres of Co_3O_4 (RT-Co_3O_4),[39] Liu et al. reported rhombus nanopillars and nanobrush arrays,[40] Chen et al. reported urchin-like Co_3O_4 hollow spheres,[41] Pal et al. reported ultra-small Co_3O_4 nanocubes,[42] etc., for capacitive performance. Also, with the same substrate, by tuning the morphology using different amounts of additive, Yu et al. reported the morphology-dependent capacitive behavior of Co_3O_4.[43] Furthermore, Xia et al. reported self-supported Co_3O_4 nanowire arrays and mesoporous Co_3O_4 monolayer hollow-sphere arrays as pseudocapacitor materials with high specific capacitance values.[44,45] However, if a self-oriented one-dimensional (1D) nanostructure can be grown directly over the current collector substrate, then it can fully exploit the redox reaction and enhance the capacitive behavior. So, keeping that in mind, in our work, we successfully prepared 1D Co_3O_4 nanowires on a flexible, conducting CF substrate. The as-prepared sample was examined in both aqueous electrolyte (three-electrode system) and a solid-state medium, that is, in a gel electrolyte (two-electrode system). By using a 3 M KOH aqueous electrolyte in the three-electrode system, we obtained a significantly high specific capacitance of 3290 F/g at a scan rate of 5 mV/s. A specific capacitance of 764 F/g at a current density of 1 A/g was achieved from the galvanostatic charge−discharge (GCD) curve. The sample showed an excellent rate capability of 93.5% after 2000 cycles. In addition, a high performance solid-state symmetric device based on CoNW/CF was meticulously designed with CoNW/CF both as the anode and cathode materials. This device delivered a highest energy and power density of 6.7 Wh/kg (0.072 mWh/cm^3) and 5000 W/kg (53.3 mW/cm^3), showing good stability under several bending conditions and after cycling for 5000 charge−discharge cycles.

RESULTS AND DISCUSSION

Vertically aligned, three-dimensionally oriented Co_3O_4 nanowires were successfully prepared by using a simple hydrothermal method, and CF as the conducting substrate was used as a growth platform. After hydrothermal reaction and postannealing treatment, the intensely black Co_3O_4 nanowire arrays covered the CF uniformly. Nucleation depends on the nature of the substrate. Generally, CFs are hydrophobic in nature, so here, by a $KMnO_4$ activation process, chemical seeding was done so that the fabric became hydrophilic and the adhesion property increased. Also, this seeding mechanism determines the morphology of the nanostructures.[46] The growth of the nanostructure is briefly illustrated in Scheme 1.

Scheme 1. Illustration of Growth of Co_3O_4 Nanowires on a Flexible CF (CoNW/CF)

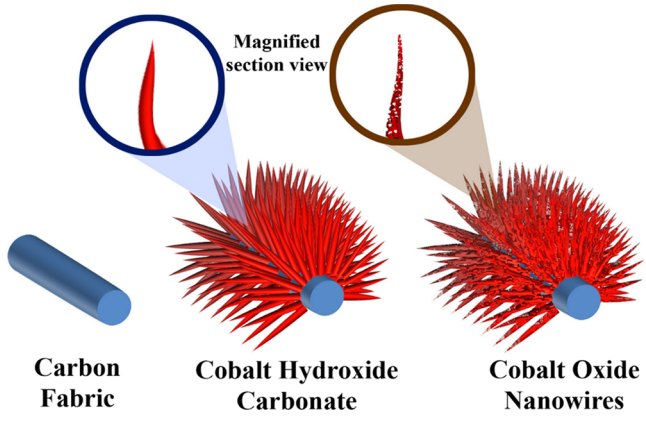

After the hydrothermal reaction, cobalt hydroxide carbonate formed over the CF, and then after annealing in air, Co_3O_4 porous nanowires formed. The detailed plausible formation mechanism of CoNW/CF has already been proposed in our previous published report.[47] Using powder X-ray diffraction (XRD), the crystallinity and phase purity of CoNW/CF was examined. As can be seen from Figure 1a, at 2θ values of 18.9, 31.3, 36.9, 44.9, 55.6, 59.5, and 65.3°, the strong and sharp diffraction peaks can be ascribed to the lattice planes of (111), (220), (311), (400), (422), (511), and (440), respectively, which corresponds well with JCPDS card no: 42-1467 of cobalt oxide. The XRD pattern also indicates good crystallinity of the as-prepared CoNW/CF. A typically broad diffraction peak at a 2θ value of 26° and a small peak at 43° are attributed to the diffraction peaks of the amorphous CF. Also, the XRD pattern marked with the lattice planes of cobalt hydroxide carbonate on CF is shown in Figure S1 in the Supporting Information.

Raman spectroscopy was carried out for the bare carbon fabric and CoNW/CF to better understand the growth of Co_3O_4 on the substrate. In the case of bare CF, there are two distinct sharp peaks observed around 1363 and 1593 cm^{-1}, which represent the well documented D and G bands of carbon materials. The Raman spectra of CoNW/CF correspond to the modes: F^1_{2g}, E_g, F^2_{2g}, F^3_{2g}, and A_{1g} of Co_3O_4 with peaks at 197, 483, 522, 621, and 693 cm^{-1}, as shown in Figure 1b, and the pattern matches well with previous reports. There were no other peaks related to the carbon material detected in the Raman spectra of CoNW/CF, which clarifies the uniform growth of the Co_3O_4 nanostructures over the CF.

In Figure 2, different magnified images explore the morphology and microstructure of the as-prepared nanostructures. The low magnification image in Figure 2a reveals that the CoNW/CF 1D nanowire array architecture uniformly covers the skeletons of each and every carbon fiber. The nanowires grow so densely that they look like the furry body of a woolly caterpillar, and the wires are almost vertical on the substrate. Also, the structures remain largely unaffected, and their morphology remains intact, even though the electrodes suffer repeated bending and twisting. The enlarged field emission scanning electron microscopy (FESEM) images in Figure 2b,c show that the nanowires are well distributed with sharp edges.

DOI: 10.1021/acsomega.7b00702
ACS Omega 2017, 2, 4216−4226

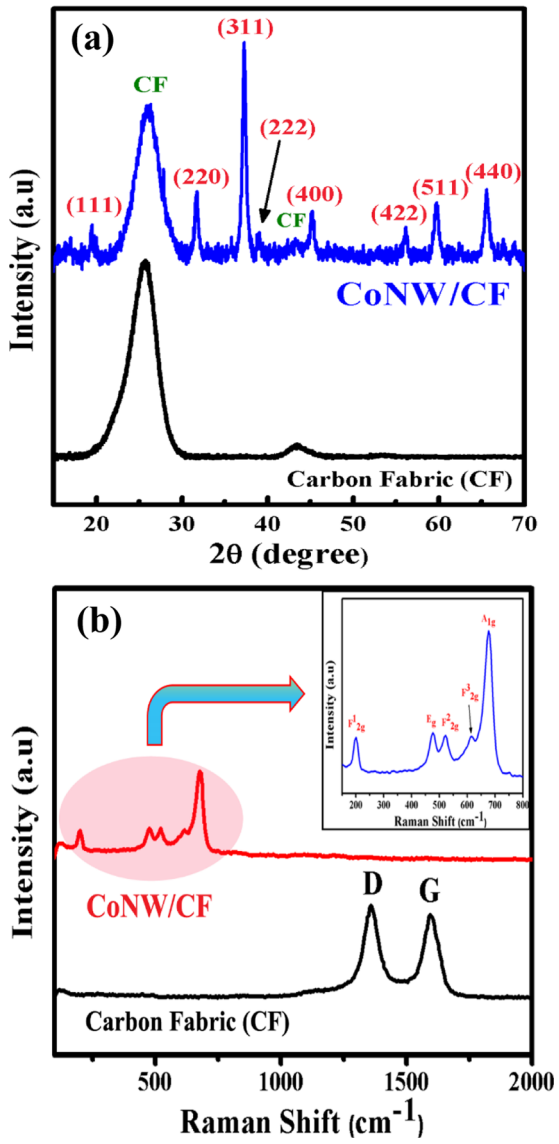

Figure 1. (a) XRD patterns of CF and CoNW/CF. The broad peak at a 2θ value of 26° is due to the graphitic nature of the CF. (b) Raman spectra of Co_3O_4 NWs on CF (CoNW/CF) and bare CF, the absence of any graphitic carbon peak indicates the uniform and dense growth of the Co_3O_4 NWs on CF. Also, in the inset, the Raman spectra of Co_3O_4 is shown.

Basically, by focused observation of the nanowires in Figure 2c, it can be clearly observed that some nanowires are mound together and have a tendency to bundle up at the top. The nanowires have a length of about 3−3.5 μm and a tip diameter of about 10−12 nm. Also, due to the decomposition of CO_2 and H_2O during annealing, porosity is created. So, these types of structures possess very high structural porosity and the surface area is significantly enhanced, which is indispensable when choosing a suitable electrode material for supercapacitors, as the number of electroactive sites can be increased due to these pores. The morphologies and microstructures were also further affirmed by the high-resolution transmission electron microscopy (HRTEM) images. The low magnification image in Figure 3a shows the fine porosity of a nanowire and that the pores are symmetrically distributed. Moreover, from the magnified image in Figure 3b, pores can be observed in the mesoscale range. This type of mesoporous architecture is more favorable for penetration of electrolyte and ionic movement to every accessible part of the nanostructure. The high resolution image in Figure 3c shows the lattice fringes, from which the *d*-spacing can be calculated to be about ∼0.28 nm, which corresponds to the (220) plane of cobalt oxide. The inset image of Figure 3c clearly shows the selected area electron diffraction (SAED) pattern in the reciprocal lattice space. The pattern illustrates the polycrystalline nature of the as-prepared CoNW/CF nanostructures. The SAED pattern of cobalt hydroxide carbonate also shows a polycrystalline nature, as shown in Figure S2. Additionally, elemental mapping by energy-dispersive X-ray spectroscopy (EDS) attached with FESEM was done to inspect the distribution of the cobalt and oxygen in a particular strand of CF, and is shown in Figure 3d−h.

Electrochemical Performance. To highlight the excellence of the as-acquired CoNW/CF nanostructures, we explored their potential application for energy storage as a supercapacitor device. The electrochemical properties were evaluated in a three-electrode configuration with a 3 M KOH aqueous electrolyte. To evaluate the pseudocapacitive characteristics, cyclic voltammetry (CV) measurements were carried out at different scan rates (5, 10, 20, 50, 100, 200, and 500 mV/s) in a potential window of −0.2 to 0.7 V (vs Ag/AgCl). Also, as the CF is the growth substrate, it is important to know if it contributes to the supercapacitive behavior. Figure S3 in the Supporting Information shows the comparative CV curves (at a scan rate 10 mV/s) of CoNW/CF and the bare CF, and it can be clearly observed that CoNW/CF exhibits much higher capacitive current than that of the bare CF. So, the total capacitance is due to the sole effect of the Co_3O_4 nanowires. CV curves of the CoNW/CF electrode measured at various scan rates are shown in Figure 4a. Each and every voltammogram profile distinctly indicate that the measured capacitance is due to surface faradic redox reactions for charge storage, and up to a scan rate of 500 mV/s, two pairs of well-designated redox peaks can be distinctly observed. These two pairs of redox peaks indicate the change of oxidation state of the Co^{2+}/Co^{3+} and Co^{3+}/Co^{4+} reversible redox couples, as shown in the following equations.[48]

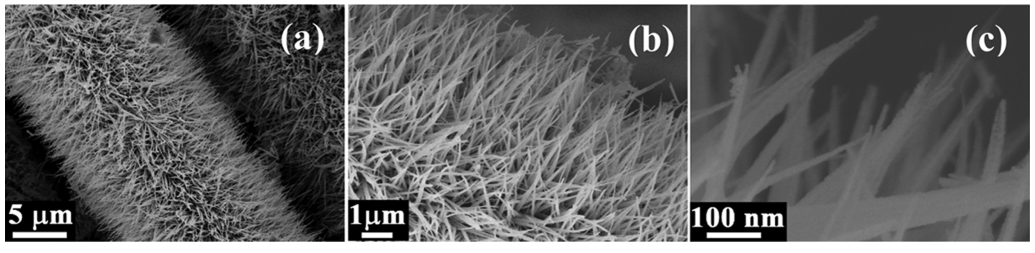

Figure 2. (a) FESEM images of CoNW/CF showing the morphology of the nanowires. (b, c) Magnified images of (a).

DOI: 10.1021/acsomega.7b00702
ACS Omega 2017, 2, 4216−4226

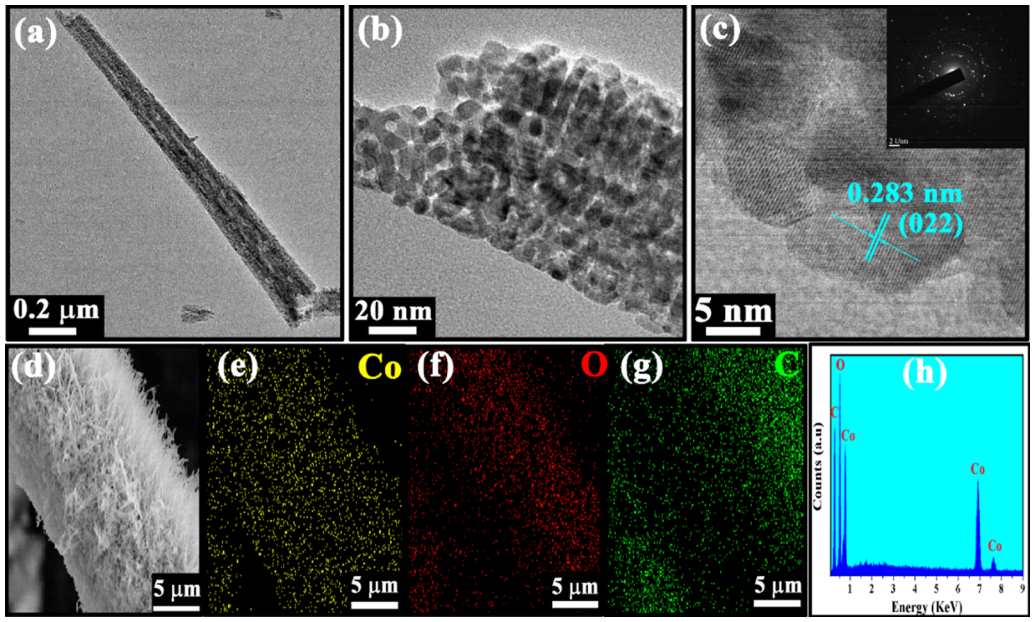

Figure 3. (a) Low magnification transmission electron microscopy (TEM) image, showing a single Co_3O_4 nanowire. (b) Higher magnification TEM image, which clearly reveals the porous nature of the nanowires. (c) Well-resolved lattice fringes with measured "*d*" value and the corresponding lattice plane. Also, the SAED pattern is shown in inset, indicating the polycrystalline nature of Co_3O_4. (d–g) EDS mapping of the constituent elements of Co_3O_4, i.e., Co and O, and C, due to CF. (h) Spectra of EDS mapping.

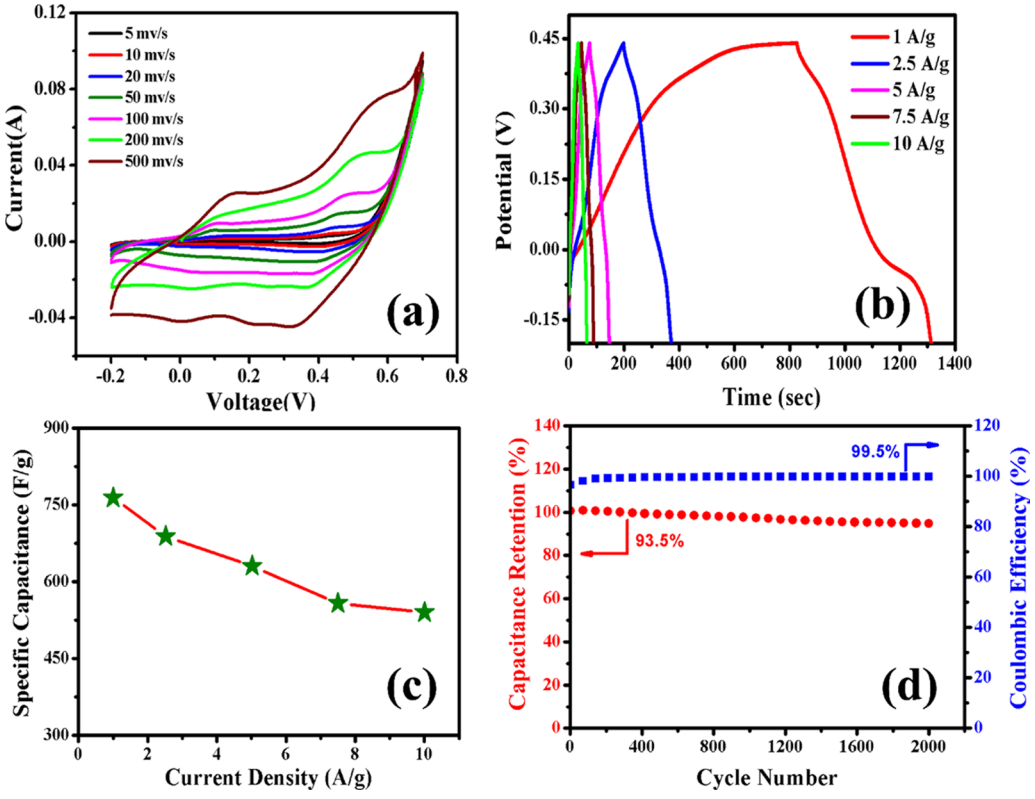

Figure 4. (a) CV and (b) GCD curves of CoNW/CF electrode in three-electrode system. (c) Obtained specific capacitance and current density plot, as calculated from GCD curve. (d) Specific capacitance retention and coulombic efficiency with cycle number.

$$Co_3O_4 + OH^- + H_2O = 3CoOOH + e^-$$

$$CoOOH + OH^- = CoO_2 + H_2O + e^-$$

With increasing scan rate from 5 to 500 mV/s, that is, after a 100-fold increase of scan rate, a slight shift of the redox peak is observed, which indicates the low resistance of the electrode and that the ions can move very fast.[36] Further details about the resistive nature of the electrode were obtained by electrochemical impedance spectroscopy (EIS) measurements. Here, we got the specific capacitance values from the CV curve by using the equation below.

DOI: 10.1021/acsomega.7b00702
ACS Omega 2017, 2, 4216−4226

$$C_s = \frac{\int I(V)\,dV}{m \times \Delta V \times \upsilon} \quad (1)$$

where $\int I(V)\,dV$ represents the area enclosed by the CV curve, m is the active mass of the electrode material, ΔV is the potential window, and υ is the scan rate. At the lowest scan rate of 5 mV/s, the obtained specific capacitance is 3290 F/g, which is significantly high and approaches the theoretical capacitance value of cobalt oxide (3650 F/g).

Figure 4b shows the GCD profile of the CoNW/CF electrode at different current densities from 1 to 10 A/g. Corresponding specific capacitance values were calculated using the following equation.

$$C_s = \frac{I \times \Delta t}{m \times \Delta V} \quad (2)$$

where I is the discharging current and Δt is the discharge time. The obtained specific capacitance values were 764, 688, 630, 558, and 540 F/g, respectively, at current densities of 1.0, 2.5, 5.0, 7.5, and 10 A/g. The corresponding graph of specific capacitance with current density is shown in Figure 4c. Although current density increases up to 10 A/g, the nanostructures retain 70.6% of their initial capacitance. Predominantly, the capacitance value decreases due to the increase of current density, as does the internal resistance of the electrode. Ions can easily penetrate and make contact with the entire electrode material at lower current density, but with increasing current density, the permeation of the ions deceases and the material at the outer surface of the electrode mainly contributes to the overall capacitance. Here, we used a CF substrate as a binder-free electrode, which itself is very conducting, so it favors ionic movement. We show a schematic picture of ion movement between the nanostructures in Figure 5. So, as a soft, flexible substrate, CF not only enables the fast

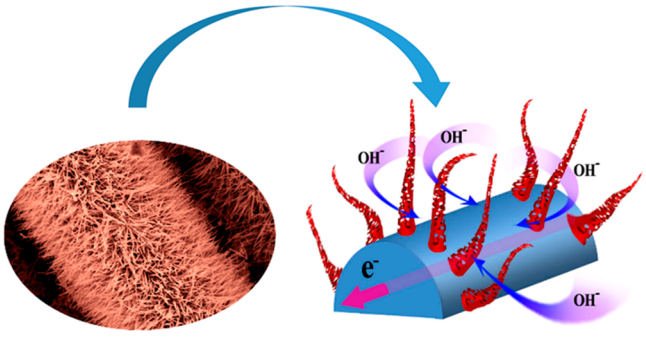

Figure 5. Schematic representation of ion movement within the porous nanowires.

electrotransport access and easy diffusion of ions, but it also eliminates the difficulties and drawbacks that arise due to the slurry-making procedure of electrode preparation with polymer binders. Cyclic stability is one of the predominant requirements for high performance supercapacitors. Figure 4d shows the capacitance retention and coulombic efficiency of the CoNW/CF electrode over 2000 cycles conducted at a current density of 10 A/g. During the 2000 charge−discharge processes, the corresponding coulombic efficiency approaches 100%, which confirms that the material, by nature, possesses good reversibility. Also, after 2000 cycles, it retains 93.5% of its initial capacitance, suggesting that the material has good electrochemical stability. Moreover, for reusability of any electrical equipment, the nanostructures of the fabricating material should retain their morphology after many cycles of operation. To verify this point, we provide the FESEM image of the nanostructure of the CoNW/CF electrode after 2000 cycles, which reveals the pristine nature of our nanostructures, in Figure S4 of the Supporting Information. However, electrochemical performance depends on many factors like the concentration of electrolyte, mass of the active material, area and thickness of the electrode, etc., and also the measuring parameters, such as the scan rates and current densities. So, on the basis of an overall study of the three-electrode system, a rough comparison with data from some reports of Co_3O_4 and Co_3O_4 composite materials is shown in Table 1 with references.

Further, the charge transfer efficiency and electrical conductivity of CoNW/CF were investigated by EIS and the electrical equivalent circuit used in fitting the experimental EIS data. The Nyquist plot of the material measured in a 3 M KOH aqueous electrolyte medium compared with a fitted curve is displayed in Figure S5a,b (Supporting Information). An inclined straight line at the low frequency region and a semicircle at the high frequency region reveal the capacitive nature of the material. The equivalent circuit is shown in the inset of Figure S5a. In the real axis, the intercept at the high frequency domain indicates the equivalent series resistance (ESR/R_s), which comprises the inherent resistance of the electroactive material, electrolyte bulk resistance, and the contact resistance that arises at the electrode/electrolyte interface. Also, from the diameter of the semicircle, we can get the contact resistance (R_{ct}), which arises due to the diffusion of the electrons. In the equivalent electrical circuit, R_1 and R_2 correspond to the ESR and the charge transfer resistance (R_{ct}), respectively. The values of R_1 and R_2 are 1.037 and 0.31 Ω. This improved electrochemical behavior can be elucidated by considering the following aspects: (1) Here, we performed the controlled growth of an electroactive material, that is, Co_3O_4 nanowires directly grown on the CF substrate, confirming good mechanical adhesion of the nanostructure with the current collector as well as providing a fast electronic transfer channel. (2) When using a polymer binder and other additives, series resistance increases and the capacitance value can be degraded. So, this issue can be eliminated here. (3) Now, last but not least is the nature of the obtained nanostructures. The unique growth of the 1D porous nanowires enables a sufficiently high surface area to facilitate penetration of the electrolyte and ion movement, which shortens the diffusion path.

Symmetric Supercapacitor (SSC) Device Performance. As the liquid electrolytic medium of the three-electrode system does not fulfill the requirements for application, we have to test the workability of CoNW/CF as a solid-state device. In symmetric configuration, both the positive and negative electrodes are made of CoNW/CF (as shown in Figure 6a) and we tested the contribution of the nanostructures in device performance without using any carbon-based materials (activated carbon, reduced graphene oxide, etc.) as the negative electrode. A digital picture in Figure S6 in the Supporting Information shows the device: two CoNW/CF layers are pasted together with a poly(vinyl alcohol) (PVA)/KOH gel electrolyte and separator. The CV and GCD curves of the CoNW/CF//CoNW/CF SSC device at different voltage windows of 0−0.6 to 0−1.0 V are shown in Figure 6b,c. We selected the input potential range up to 1.0 V to further investigate the device performance. Within this voltage limit,

DOI: 10.1021/acsomega.7b00702
ACS Omega 2017, 2, 4216−4226

Table 1. Comparison on the Basis of the Three-Electrode System

work	electrolyte used	specific capacitance (F/g) at scan rate (mV/s)	specific capacitance (F/g) at current density (A/g)	long cycle and capacitance retention	refs
ultrafine Co_3O_4 nanocrystal	0.5 M H_3PO_4	1049 F/g at 1 mV/s	762 F/g at 6 A/g		49
Co_3O_4/CNF	6 M KOH		586 F/g at 1 A/g	74% after 2000 cycles	50
CoO rhombus nanopillar/nanobrush	2 M KOH	509 F/g at 10 mV/s			40
$Co_3O_4/ZnFe_2O_4$	6 M KOH		326 F/g at 1 A/g	80.7% after 1000 cycles	51
$Co_3O_4@Co_3S_4$	3 M KOH	1284 F/g at 2 mV/s		93.1% after 5000 cycles	52
HCCA(3)/Co_3O_4	1 M KOH	435 F/g at 10 mV/s	456 F/g at 1 A/g	89% after 2000 cycles	53
freestanding Co_3O_4 nanowire	2 M KOH		754 F/g at 2 A/g		54
Cd doped porous Co_3O_4	6 M KOH		737 F/g at 1 A/g	96% after 1000 cycles	55
Co_3O_4 nanosheet@nanowire	1 M KOH		715 F/g	100% after 1000 cycles	56
urchin-like Co_3O_4	3 M KOH		614 F/g at 1 A/g	77% after 5000 cycles	57
RT-Co_3O_4	3 M KOH	1324 F/g at 5 mV/s	219 F/g at 1 A/g	95% after 4000 cycles	39
porous Co_3O_4 microflowers	3 M KOH		240.2 F/g at 0.625 A/g	96.3% after 2000 cycles	58
PSAC/Co_3O_4	1 M KOH	80 F/g at 2 mV/s	94 F/g at 1 A/g	88% after 1000 cycles	59
needle-like Co_3O_4/GO	2 M KOH		157.7 F/g at 0.1 A/g	70% after 4000 cycles	60
three-dimensional (3D)-nanonet hollow structured Co_3O_4	6 M KOH	820 F/g at 5 mV/s	739 F/g at 1 A/g	90.2% after 1000 cycles	61
CoNW/CF	3 M KOH	3290 F/g at 5 mV/s	764 F/g at 1 A/g	93.5% after 2000 cycles	this work

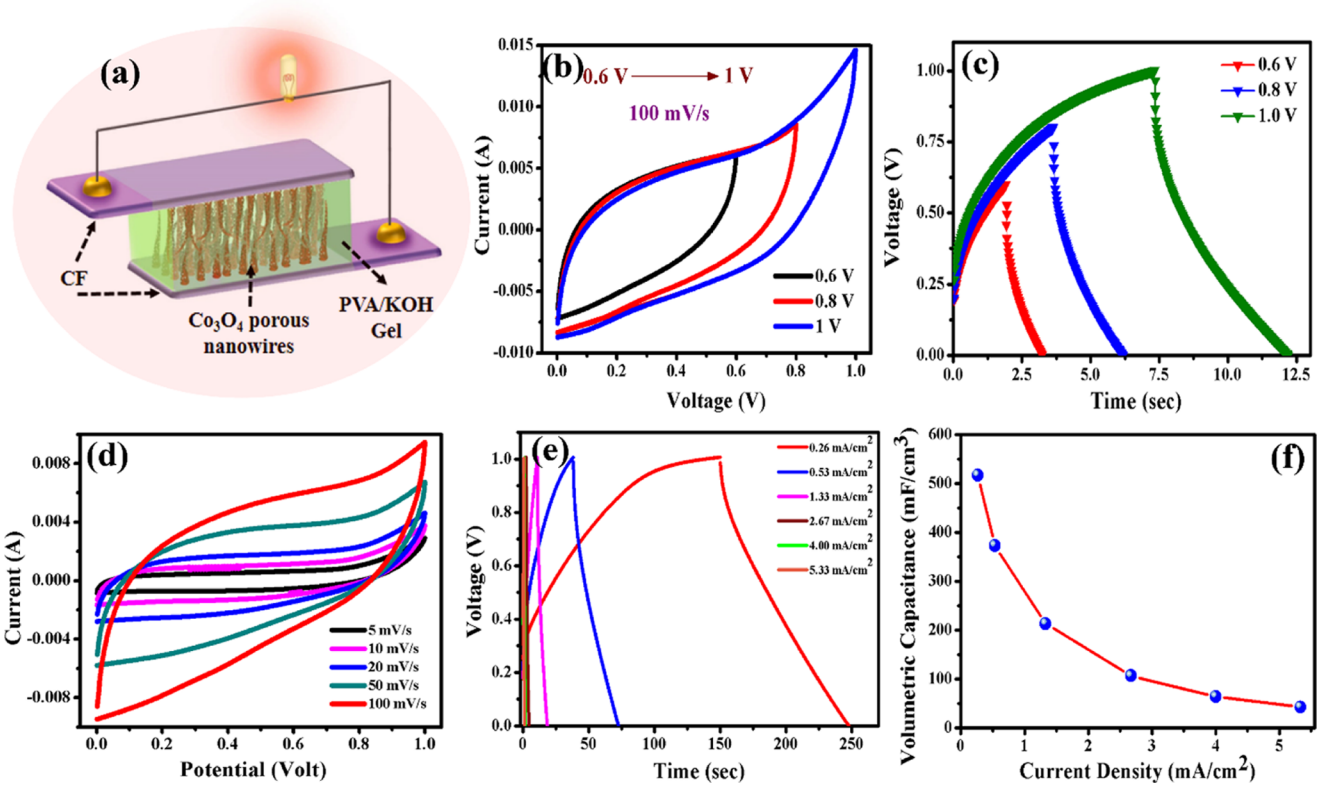

Figure 6. (a) Simplistic illustration of the SSC device that consisted of two CoNW/CF layers as the positive and negative electrodes with PVA/KOH gel electrolyte. (b) CV and (c) GCD profiles collected at different voltage windows. (d) CV at different scan rates and (e) GCD profiles at different current densities measured at a voltage window 0−1 V. (f) Volumetric capacitance vs current density plot.

the CV curves maintain a quasi-rectangular shape, which indicates that the CoNW/CF//CoNW/CF SSC device shows ideal capacitive behavior. Also, the CV curves at different scan rates (5−100 mV/s) in voltage window 0−1 V are shown in Figure 6d. With increasing scan rate, the CV curves retain their quasi-rectangular shape without any redox peak, which implies that the fabricated device performs as an EDLC. Figure 6e shows the charging−discharging profile of the as-prepared SSC device at different current densities (0.26−5.33 mA/cm^2). When designing a device, the area and volume of the electrodes are the prime parameters to get a desired areal or volumetric capacitance. We get a remarkably high volumetric capacitance for our SSC device. The device provides a maximum volumetric capacitance of 517.33 mF/cm^3 at a current density of 0.26 mA/cm^2, and retains a capacitance value of 43.6 mF/cm^3 even at a high current density of 5.3 mA/cm^2. The required formulae for calculating volumetric capacitance are given in the Supporting Information. These results show good rate capability. Also,

DOI: 10.1021/acsomega.7b00702
ACS Omega 2017, 2, 4216−4226

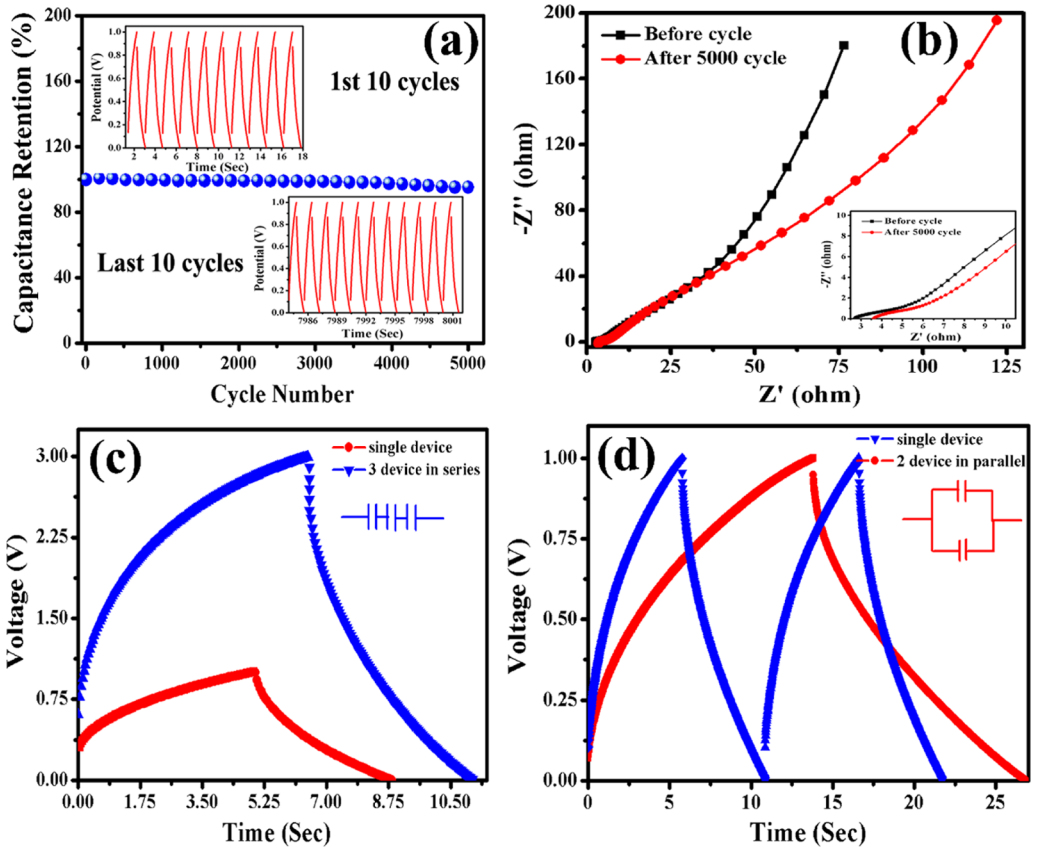

Figure 7. (a) Cyclic performance of SSC device at a current density of 4 mA/cm^2 for 5000 cycles, inset depicts first and final 10 charging−discharging profiles. (b) Electrochemical impedance spectra of SSC device before and after 5000 cycles. (c, d) Charging−discharging profile of one single SSC device, three SSC devices connected in series, and two SSC devices connected in parallel, showing similar characteristics to a capacitor.

cyclic performance is one of the crucial parameters in the field of practical application, so the cycling lifetime of the CoNW/CF//CoNW/CF SSC device was examined at a current density of 4 mA/cm^2 within a potential window of 0.0−1.0 V. The obtained result shown in Figure 7a is exceptionally good, confirming long-term cyclic stability. The device retains 95.3% of its initial capacitance after 5000 charging−discharging cycles, and the 1st and last 10 cycles are displayed in the graph (as insets of Figure 7a), indicating the outstanding stability of the device. The obtained result is much superior to some recent reports on CF.[31] Also, Yu et al. reported manganese oxide nanorods on CF and their symmetric device showed 76.5% capacitance retention after 5000 cycles,[62] Jagadale et al. published their symmetric $Co(OH)_2$−$Co(OH)_2$ supercapacitor, which retained 81% initial capacitance after 5000 cycles,[63] and Hu et al. reported a SSC of 3D Co_3O_4@NiO hierarchical nanowire arrays with a capacitance retention of 91.35% after 5000 cycles.[64] So, as a SSC, our fabricated device has remarkably good cyclic stability. EIS study verified whether electronic movement is feasible in our device. Figure 7b shows the EIS plot of the as-prepared CoNW/CF//CoNW/CF SSC device before cyclic performance as well as after 5000 cycles. The inclined line in the low frequency region is nearly parallel to the imaginary axis, which confirms that the device tends toward an ideal capacitive nature. The ESR that we get from the intercept of the real axis at the high frequency region is 2.8 Ω, which implies a charge transfer process, and after 5000 cycles, this value increases slightly to 3.6 Ω. So, although we use a gel electrolyte, the device is not so resistive, even after long-term cyclic performance. Also, the capacitive behavior was ensured by employing the device in some series and parallel combinations. Figure 7c,d shows the results of the charge−discharge profiles of three devices connected in series, and two devices in parallel, respectively. The obtained results match well with the nature of a capacitor. Some discrepancy observed in the charging and discharging time may be due to the slight amount of mass change between the two or three different devices.

To investigate the potential applicability of the SSC device, electrochemical performance analysis was conducted under mechanical bending conditions to ensure its flexibility. The cyclic voltammetric performance of the device at a scan rate of 50 mV/s was observed under bending conditions and was found to be the same as that under its normal configuration. The obtained curves are shown in Figure S7 in the Supporting Information.

Figure S8 in the Supporting Information displays the gravimetric ragone plot of our SSC device. The maximum energy density that we get for our device is 0.071 mWh/cm^3 at a power density of 2.66 mW/cm^3 (6.7 Wh/kg at 248.65 W/kg) and the maximum power density is 54 mW/cm^3 at 0.006 mWh/cm^3 (5000 W/kg at 0.55 Wh/kg). Calculation of power and energy density is given in the Supporting Information. To further illustrate the practical use of the CoNW/CF//CoNW/CF SSC device, four CoNW/CF//CoNW/CF SSCs were connected in series, and were able to light up a combination (series) of five light-emitting diodes (LEDs) (as shown in Figure 8a). This series combination of four SSC devices

DOI: 10.1021/acsomega.7b00702
ACS Omega 2017, 2, 4216−4226

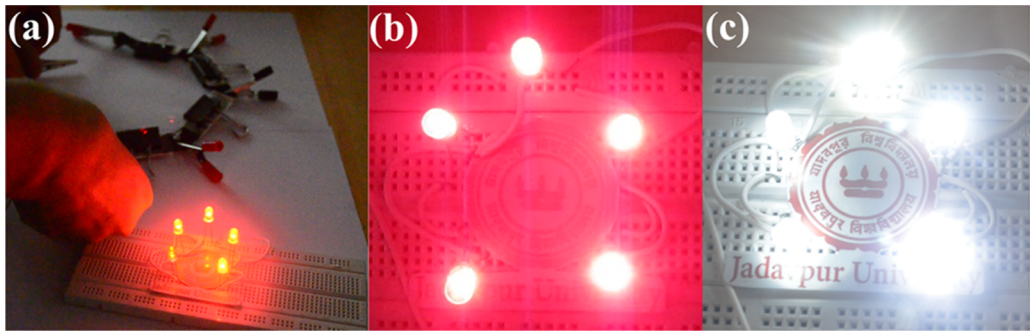

Figure 8. (a) Digital photographs of glowing LEDs with SSC devices connected in series. Photographs of (b) five glowing red LEDs and (c) five glowing white LEDs connected in series. Photograph courtesy of Promita Howli. Copyright 2017.

provided a voltage window of 4 V, and after charging for 5 s, it was able to light up the series of five red LEDs for 1 min (Figure 8b). Due to its high power density, the device was able to light up a combination (series) of five white light LEDs (Figure 8c, Video).

CONCLUSIONS

In summary, an ecofriendly, cost-effective simple chemical method has been demonstrated to fabricate CoNW/CF, and this material was used as a binder-free electrode for supercapacitor application. The as-prepared nanostructures exhibit a significantly high specific capacitance of 3290 F/g at a scan rate of 5 mV/s, which is very close to the theoretical capacitance value of cobalt oxide. This high capacitance value is attributed to the highly ordered 3D coaxial nanostructures on the conductive CF substrate. Here, the CF facilitates electron transportation and also enables application in the field of flexible electronics. Moreover, a symmetric solid-state device was prepared by using two CoNW/CF layers as positive and negative electrodes, which achieved a good energy density of 0.071 mWh/cm^3 at a power density of 2.66 mW/cm^3 (6.7 Wh/kg at 248.65 W/kg) and a power density of 54 mW/cm^3 at 0.006 mWh/cm^3 (5000 W/kg at 0.55 Wh/kg). It is noteworthy that our fabricated device showed excellent cyclic stability and retained 93.5% of its initial capacitance after cycling for 5000 times. As a practical demonstration, CoNW/CF//CoNW/CF SSC devices connected in series were able to supply sufficient energy and power to light up a series of LEDs. This work comprises the first demonstration of CoNW/CF used as a symmetric solid-state supercapacitor, with improved performance for next-generation high performance flexible energy storage devices.

EXPERIMENTAL SECTION

Materials. Cobalt nitrate ($Co(NO_3)_2$) and ammonium fluoride (NH_4F) were purchased from Sigma-Aldrich and urea ($CO(NH_2)_2$), potassium permanganate ($KMnO_4$), KOH, and conc. H_2SO_4 were of analytical grade and used as received without further purification. Deionized (DI) water obtained from a Millipore water purification plant was used throughout the experiment.

Synthesis of CoNW/CF. CoNW/CF was synthesized in a similar way to that reported in our previous paper,[47] which is briefly described as follows: Commercially available CF was used as a supporting substrate material for the growth of the Co_3O_4 nanowires. First of all, the CF was cleaned by ultrasonication in acetone and subsequently DI water. Prior to deposition, the CF substrate was chemically activated with $KMnO_4$. As this is a liquid phase technique, it overcomes the other difficulties that arise in the case of physical deposition. Additionally, for growth on large area substrates, this technique is much more compatible. A 100 mL nutrient solution was prepared by mixing three independently prepared solutions: 50 mL of 50 mM $Co(NO_3)_2{\cdot}6H_2O$, 30 mL of 100 mM NH_4F, and 20 mL of 250 mM urea solutions, respectively. The obtained homogeneous pink solution was transferred into a 100 mL stainless steel autoclave and the seeded CF was mounted on a glass slide and inserted in an oblique manner into the solution, keeping the activated surface down, which avoided bulk precipitation, and also the surface facing down acted as a growth platform. Then, the sealed autoclave was kept in a hot air oven at 120 °C for 6 h. After the hydrothermal reaction, the autoclave was left to cool down naturally at room temperature. The obtained pink colored CF was washed several times in a flow of doubly distilled water and lastly with ethanol to remove impurities. After drying at 80 °C, the deposited substrate was annealed in a muffle furnace at 400 °C for 3 h at a heating rate of 5 °C/min. Finally, the intense black-colored CF was obtained, indicating the formation of the Co_3O_4 nanostructures. The mass of the active material was measured from the weight difference of the pure CF and the electrode obtained after the growth of Co_3O_4 nanostructures.

CHARACTERIZATION

The composition and crystallinity of the as-synthesized sample were characterized by X-ray diffractometry (Bruker D8 Advance) employing Cu Kα radiation (λ = 1.5406 Å), operating at 40 kV and 40 mA in a 2θ range of 20−80°. Raman spectra were obtained using a confocal Raman spectrometer (laser source of λ = 532 nm, alpha300; Witec, Germany). The morphologies and microstructures of the nanowires were inspected by FESEM (operated at 5 kV, S-4800; Hitachi) and also EDS (Thermo Scientific attached with Hitachi S-4800 operated at 15 kV) was used as a characterization tool for spectral elemental analysis and determination of stoichiometry. The microstructure was examined in more detail, as well as the lattice spacing and SAED pattern, by HRTEM (operated at 200 kV, JEM 2100; JEOL, Ltd.).

Electrochemical Measurements. All electrochemical measurements, namely, CV, GCD, and EIS, were conducted in a three-electrode cell of Gamry Interface 1000 (potentiostat/galvanostat/ZRA). Here, CoNW/CF (1 cm^2 area) was used directly as the working electrode; the portion of CF supported by electroactive material was immersed into the electrolyte keeping the bare portion outside for electrical connection. A platinum wire and Ag/AgCl electrode were used as the counter

DOI: 10.1021/acsomega.7b00702
ACS Omega 2017, 2, 4216−4226

and reference electrode, respectively. Measurements were taken in 3 M KOH aqueous electrolyte. The working potential window was −0.2 to 0.7 V with various scan rates in the range of 5−500 mV/s for typical CV curves, and GCD was measured at a current density of 1−10 A/g. EIS measurements were performed in a frequency range of 0.01 Hz to 1 MHz.

Fabrication of an All Solid-State SSC Device. The solid-state SSC device was fabricated by assembling two pieces of CoNW/CF (as the positive and negative electrode) with PVA/KOH gel electrolyte and Whatman filter paper as a separator. First of all, the gel electrolyte was obtained as follows: 3 g of PVA and 1.5 g of KOH were put in 30 mL of DI water, and the mixture was stirred vigorously with increasing temperature. Then, the temperature was fixed at 90 °C, and stirring was continued until the solution became clear and homogeneous. Gel formation took place after about 1.5 h, and then it was left for some time without heating and stirring to eliminate the excess bubbles that formed during dissolution. After that, the two pieces of CoNW/CF were dipped into the gel electrolyte keeping the un-deposited portion of the CF outside. Also, the filter paper was soaked in the gel, and then the electrodes and the separator were dried at room temperature to evaporate the excess water. Finally, the two pieces of CoNW/CF were assembled with filter paper between them. The electrochemical characteristics of that cell were also tested at the same electrochemical workstation (Gamry Interface 1000, Potentiostat/Galvanostat/ZRA)

■ ASSOCIATED CONTENT

Supporting Information

The Supporting Information is available free of charge on the ACS Publications website at DOI: 10.1021/acsomega.7b00702.

XRD patterns of cobalt hydroxide carbonate; SAED pattern of cobalt hydroxide carbonate; CV curve of CoNW/CF electrode and bare CF at a scan rate of 10 mV/s; FESEM image of CoNW/CF electrode after 2000 cycles; Nyquist plot of CoNW/CF electrode with fitted circuit; pictorial image of as-prepared SSC device; CV curve of SSC device at normal conditions and bending conditions at a scan rate of 50 mV/s; gravimetric ragone plot of the SSC device and the additional formulae (PDF)

Web-Enhanced Feature

Video of a combination of LEDs in operation using the SSC devices

■ AUTHOR INFORMATION

Corresponding Author

*E-mail: kalyan_chattopadhyay@yahoo.com. Tel: +91 33 2413 8917. Fax: +91 33 2414 6007.

ORCID

Kalyan Kumar Chattopadhyay: 0000-0002-4576-2434

Present Addresses

[§]Department of Physics, Prabhu Jagatbandhu College, Jhorhat, Andul, Howrah 711302, India (P.H.).

[∥]Department of Basic Science and Humanities, Techno India - Batanagar, Kolkata 700141, India (N.S.D.).

Notes

The authors declare no competing financial interest.

■ ACKNOWLEDGMENTS

P.H. would like to thank the University Grants Commission (UGC), Government of India, for awarding her a junior research fellowship during the execution of the research work. We are also thankful to the UGC for the "University with Potential for Excellence (UPE-II)" scheme and DST PURSE-II.

■ REFERENCES

(1) Winter, M.; Brodd, R. J. What are batteries, fuel cells, and supercapacitors? *Chem. Rev.* **2004**, *104*, 4245−4270.

(2) Kang, B.; Ceder, G. Battery materials for ultrafast charging and discharging. *Nature* **2009**, *458*, 190−193.

(3) Tarascon, J.-M.; Armand, M. Issues and challenges facing rechargeable lithium batteries. *Nature* **2001**, *414*, 359−367.

(4) Xiao, X.; Peng, X.; Jin, H.; Li, T.; Zhang, C.; Gao, B.; Hu, B.; Huo, K.; Zhou, J. Freestanding mesoporous VN/CNT hybrid electrodes for flexible all-solid-state supercapacitors. *Adv. Mater.* **2013**, *25*, 5091−5097.

(5) Xiao, X.; Li, T.; Yang, P.; Gao, Y.; Jin, H.; Ni, W.; Zhan, W.; Zhang, X.; Cao, Y.; Zhong, J.; Gong, L.; Yen, W.-C.; Mai, W.; Chen, J.; Huo, K.; Chueh, Y.-L.; Wang, Z. L.; Zhou, J. Fiber-based all-solid-state flexible supercapacitors for self-powered systems. *ACS Nano* **2012**, *6*, 9200−9206.

(6) Lin, H.; Li, L.; Ren, J.; Cai, Z.; Qiu, L.; Yang, Z.; Peng, H. Conducting polymer composite film incorporated with aligned carbon nanotubes for transparent, flexible and efficient supercapacitor. *Sci. Rep.* **2013**, *3*, No. 1353.

(7) Mai, L.; Tian, X.; Xu, X.; Chang, L.; Xu, L. Nanowire electrodes for electrochemical energy storage devices. *Chem. Rev.* **2014**, *114*, 11828−11862.

(8) Mai, L.; Li, H.; Zhao, Y.; Xu, L.; Xu, X.; Luo, Y.; Zhang, Z.; Ke, W.; Niu, C.; Zhang, Q. Fast ionic diffusion-enabled nanoflake electrode by spontaneous electrochemical pre-intercalation for high-performance supercapacitor. *Sci. Rep.* **2013**, *3*, No. 1718.

(9) Tao, J.; Liu, N.; Ma, W.; Ding, L.; Li, L.; Su, J.; Gao, Y. Solid-state high performance flexible supercapacitors based on polypyrrole-MnO_2-carbon fiber hybrid structure. *Sci. Rep.* **2013**, *3*, No. 2286.

(10) Giri, S.; Ghosh, D.; Das, C. K. Growth of Vertically Aligned Tunable Polyaniline on Graphene/ZrO_2 Nanocomposites for Supercapacitor Energy-Storage Application. *Adv. Funct. Mater.* **2014**, *24*, 1312−1324.

(11) An, L.; Yu, L.; Cao, Y.; Li, W.; Xu, K.; Ji, T.; Zou, R.; Hu, J. Hierarchical architectures of Co_3O_4 ultrafine nanowires grown on Co_3O_4 nanowires with fascinating electrochemical performance. *New J. Chem.* **2016**, *40*, 377−384.

(12) Calvo, E. G.; Lufrano, F.; Staiti, P.; Brigandì, A.; Arenillas, A.; Menéndez, J. A. Optimizing the electrochemical performance of aqueous symmetric supercapacitors based on an activated carbon xerogel. *J. Power Sources* **2013**, *241*, 776−782.

(13) Gao, Y.; Pandey, G. P.; Turner, J.; Westgate, C. R.; Sammakia, B. Chemical vapor-deposited carbon nanofibers on carbon fabric for supercapacitor electrode applications. *Nanoscale Res. Lett.* **2012**, *7*, 651.

(14) de Morais, E. A.; Alvial, G.; Longuinhos, R.; Figueiredo, J. M. A.; Lacerda, R. G.; Ferlauto, A. S.; Ladeira, L. O. Enhanced electrochemical activity using vertically aligned carbon nanotube electrodes grown on carbon fiber. *Mater. Res.* **2011**, *14*, 403−407.

(15) Jin, H.; Wang, X.; Gu, Z.; Anderson, G.; Muthukumarappan, K. Distillers dried grains with soluble (DDGS) bio-char based activated carbon for supercapacitors with organic electrolyte tetraethylammonium tetrafluoroborate. *J. Environ. Chem. Eng.* **2014**, *2*, 1404−1409.

(16) Liu, W.-W.; Yan, X.-B.; Lang, J.-W.; Peng, C.; Xue, Q.-J. Flexible and conductive nanocomposite electrode based on graphene sheets and cotton cloth for supercapacitor. *J. Mater. Chem.* **2012**, *22*, 17245−17253.

(17) Liu, W.-W.; Yan, X.-B.; Lang, J.-W.; Pu, J.-B.; Xue, Q.-J. Supercapacitors based on graphene nanosheets using different non-aqueous electrolytes. *New J. Chem.* **2013**, *37*, 2186−2195.

DOI: 10.1021/acsomega.7b00702
ACS Omega 2017, 2, 4216−4226

(18) Duay, J.; Sherrill, S. A.; Gui, Z.; Gillette, E.; Lee, S. B. Self-limiting electrodeposition of hierarchical MnO_2 and M $(OH)_2/MnO_2$ nanofibril/nanowires: mechanism and supercapacitor properties. *ACS Nano* **2013**, *7*, 1200−1214.
(19) Vinny, R. T.; Chaitra, K.; Venkatesh, K.; Nagaraju, N.; Kathyayini, N. An excellent cycle performance of asymmetric supercapacitor based on bristles like α-MnO_2 nanoparticles grown on multiwalled carbon nanotubes. *J. Power Sources* **2016**, *309*, 212−220.
(20) Hu, C.-C.; Chang, K.-H.; Lin, M.-C.; Wu, Y.-T. Design and tailoring of the nanotubular arrayed architecture of hydrous RuO_2 for next generation supercapacitors. *Nano Lett.* **2006**, *6*, 2690−2695.
(21) Shinde, S. K.; Dubal, D. P.; Ghodake, G. S.; Fulari, V. J. Hierarchical 3D-flower-like CuO nanostructure on copper foil for supercapacitors. *RSC Adv.* **2015**, *5*, 4443−4447.
(22) Shinde, S. K.; Dubal, D. P.; Ghodake, G. S.; Gomez-Romero, P.; Kim, S.; Fulari, V. J. Influence of Mn incorporation on the supercapacitive properties of hybrid $CuO/Cu(OH)_2$ electrodes. *RSC Adv.* **2015**, *5*, 30478−30484.
(23) Moosavifard, S. E.; El-Kady, M. F.; Rahmanifar, M. S.; Kaner, R. B.; Mousavi, M. F. Designing 3D highly ordered nanoporous CuO electrodes for high-performance asymmetric supercapacitors. *ACS Appl. Mater. Interfaces* **2015**, *7*, 4851−4860.
(24) Saravanakumar, B.; Purushothaman, K. K.; Muralidharan, G. Interconnected V_2O_5 nanoporous network for high-performance supercapacitors. *ACS Appl. Mater. Interfaces* **2012**, *4*, 4484−4490.
(25) Yoon, S.; Kang, E.; Kim, J. K.; Lee, C. W.; Lee, J. Development of high-performance supercapacitor electrodes using novel ordered mesoporous tungsten oxide materials with high electrical conductivity. *Chem. Commun.* **2011**, *47*, 1021−1023.
(26) Cai, Y.; Wang, Y.; Deng, S.; Chen, G.; Li, Q.; Han, B.; Han, R.; Wang, Y. Graphene nanosheets-tungsten oxides composite for supercapacitor electrode. *Ceram. Int.* **2014**, *40*, 4109−4116.
(27) Ren, X.; Guo, C.; Xu, L.; Li, T.; Hou, L.; Wei, Y. Facile synthesis of hierarchical mesoporous honeycomb-like NiO for aqueous asymmetric Supercapacitors. *ACS Appl. Mater. Interfaces* **2015**, *7*, 19930−19940.
(28) Shen, M.; Ma, L.; Zhu, J.; Li, X.; Wang, C. An assembled-nanosheets discus-like $Ni(OH)_2$ hierarchical structure as a high performance electrode material for supercapacitors. *RSC Adv.* **2015**, *5*, 59659−59664.
(29) Sun, B.; He, X.; Leng, X.; Jiang, Y.; Zhao, Y.; Suo, H.; Zhao, C. Flower-like polyaniline−NiO structures: a high specific capacity supercapacitor electrode material with remarkable cycling stability. *RSC Adv.* **2016**, *6*, 43959−43963.
(30) Bai, M.-H.; Liu, T.-Y.; Luan, F.; Li, Y.; Liu, X.-X. Electrodeposition of vanadium oxide−polyaniline composite nanowire electrodes for high energy density supercapacitors. *J. Mater. Chem. A* **2014**, *2*, 10882−10888.
(31) Kong, D.; Ren, W.; Cheng, C.; Wang, Y.; Huang, Z.; Yang, H. Y. Three-dimensional $NiCo_2O_4$@Polypyrrole coaxial nanowire arrays on carbon textiles for high-performance flexible asymmetric solid-state Supercapacitor. *ACS Appl. Mater. Interfaces* **2015**, *7*, 21334−21346.
(32) Wang, Q.; Wang, X.; Liu, B.; Yu, G.; Hou, X.; Chen, D.; Shen, G. $NiCo_2O_4$ nanowire arrays supported on Ni foam for high-performance flexible all-solid-state supercapacitors. *J. Mater. Chem. A* **2013**, *1*, 2468−2473.
(33) Liao, Q.; Li, N.; Cui, H.; Wang, C. Vertically-aligned graphene@MnO nanosheets as binder-free high-performance electrochemical pseudocapacitor electrodes. *J. Mater. Chem. A* **2013**, *1*, 13715−13720.
(34) Qian, Y.; Liu, R.; Wang, Q.; Xu, J.; Chen, D.; Shen, G. Efficient synthesis of hierarchical NiO nanosheets for high-performance flexible all-solid-state supercapacitors. *J. Mater. Chem. A* **2014**, *2*, 10917−10922.
(35) Jabeen, N.; Xia, Q.; Yang, M.; Xia, H. Unique core-shell nanorod arrays with polyaniline deposited into mesoporous $NiCo_2O_4$ support for high-performance supercapacitor electrodes. *ACS Appl. Mater. Interfaces* **2016**, *8*, 6093−6100.
(36) Huang, Z.; Zhang, Z.; Qi, X.; Ren, X.; Xu, G.; Wan, P.; Sun, X.; Zhang, H. Wall-like hierarchical metal oxide nanosheet arrays grown on carbon cloth for excellent supercapacitor electrodes. *Nanoscale* **2016**, *8*, 13273−13279.
(37) Liao, Q. Y.; Li, S. Y.; Cui, H.; Wang, C. Vertically-aligned graphene@Mn_3O_4 nanosheets for a high-performance flexible all-solid-state symmetric supercapacitor. *J. Mater. Chem. A* **2016**, *4*, 8830−8836.
(38) Yang, Q.; Lu, Z.; Sun, X.; Liu, J. Ultrathin Co_3O_4 nanosheet arrays with high supercapacitive performance. *Sci. Rep.* **2013**, *3*, No. 3537.
(39) Shim, H.-W.; Lim, A.-H.; Kim, J.-C.; Jang, E.; Seo, S.-D.; Lee, G.-H.; Kim, T.-D.; Kim, D.-W. Scalable one-pot bacteria-templating synthesis route toward hierarchical, porous-Co_3O_4 superstructures for supercapacitor electrodes. *Sci. Rep.* **2013**, *3*, No. 2325.
(40) Liu, Y.-B.; Lin, L.-Y.; Huang, Y.-Y.; Tu, C.-C. Investigation of the electroactive capability for the supercapacitor electrode with cobalt oxide rhombus nanopillar and nanobrush arrays. *J. Power Sources* **2016**, *315*, 23−34.
(41) Chen, F.; Liu, X.; Zhang, Z.; Zhang, N.; Pan, A.; Liang, S.; Ma, R. Controllable fabrication of urchin-like Co_3O_4 hollow spheres for high-performance supercapacitors and lithium-ion batteries. *Dalton Trans.* **2016**, *45*, 15155−15161.
(42) Pal, M.; Rakshit, R.; Singh, A. K.; Mandal, K. Ultra high supercapacitance of ultra small Co_3O_4 nanocubes. *Energy* **2016**, *103*, 481−486.
(43) Yu, Z.; Cheng, Z.; Tai, Z.; Wang, X.; Subramaniyam, C. M.; Fang, C.; Al-Rubaye, S.; Wang, X.; Dou, S. Tuning the morphology of Co_3O_4 on Ni foam for supercapacitor application. *RSC Adv.* **2016**, *6*, 45783−45790.
(44) Xia, X.-H.; Tu, J.-P.; Mai, Y.-J.; Wang, X.-L.; Gu, C.-D.; Zhao, X.-B. Self-supported hydrothermal synthesized hollow Co_3O_4 nanowire arrays with high supercapacitor capacitance. *J. Mater. Chem.* **2011**, *21*, 9319−9325.
(45) Xia, X.-H; Tu, J.-P.; Wang, X.-L.; Gu, C.-D.; Zhao, X.-B. Mesoporous Co_3O_4 monolayer hollow-sphere array as electrochemical pseudocapacitor material. *Chem. Commun.* **2011**, *47*, 5786−5788.
(46) Panigrahi, K.; Das, S.; Saha, S.; Das, B.; Sen, D.; Howli, P.; Chattopadhyay, K. K. Chemically activated growth of CuO nanostructures for flexible cold cathode emission. *CrystEngComm* **2016**, *18*, 3389−3398.
(47) Howli, P.; Das, S.; Saha, S.; Das, B.; Hazra, P.; Sen, D.; Chattopadhyay, K. K. RGO enveloped vertically aligned Co_3O_4 nanowires on carbon fabric: a highly efficient prototype for flexible field emitter arrays. *RSC Adv.* **2016**, *6*, 91860−91869.
(48) Liao, Q.; Li, N.; Jin, S.; Yang, G.; Wang, C. All-solid-state symmetric supercapacitor based on Co_3O_4 nanoparticles on vertically aligned graphene. *ACS Nano* **2015**, *9*, 5310−5317.
(49) Liu, X. Y.; Gao, Y. Q.; Yang, G. W. A flexible, transparent and super-long-life supercapacitor based on ultrafine Co_3O_4 nanocrystal electrodes. *Nanoscale* **2016**, *8*, 4227−4235.
(50) Abouali, S.; Garakani, M. A.; Zhang, B.; Xu, Z.-L.; Heidari, E. K.; Huang, J.-Q.; Huang, J.; Kim, J.-K. Electrospun carbon nanofibers with in situ encapsulated Co_3O_4 nanoparticles as electrodes for high-performance supercapacitors. *ACS Appl. Mater. Interfaces* **2015**, *7*, 13503−13511.
(51) Hu, X.-W.; Liu, S.; Qu, B.-T.; You, X.-Z. Starfish-shaped $Co_3O_4/ZnFe_2O_4$ hollow nanocomposite: synthesis, supercapacity, and magnetic properties. *ACS Appl. Mater. Interfaces* **2015**, *7*, 9972−9981.
(52) Liu, B.; Kong, D.; Zhang, J.; Wang, Y.; Chen, T.; Cheng, C.; Yang, H. Y. 3D hierarchical Co_3O_4@Co_3S_4 nanoarrays as cathode materials for asymmetric pseudocapacitors. *J. Mater. Chem. A* **2016**, *4*, 3287−3296.
(53) Kim, M.; Oh, I.; Ju, H.; Kim, J. Introduction of Co_3O_4 into activated honeycomb-like carbon for the fabrication of high performance electrode materials for supercapacitors. *Phys. Chem. Chem. Phys.* **2016**, *18*, 9124−9132.
(54) Xia, X.-H.; Tu, J.-P.; Zhang, Y.-Q.; Mai, Y.-J.; Wang, X.-L.; Gu, C.-D.; Zhao, X.-B. Freestanding Co_3O_4 nanowire array for high performance supercapacitors. *RSC Adv.* **2012**, *2*, 1835−1841.

DOI: 10.1021/acsomega.7b00702
ACS Omega 2017, 2, 4216−4226

(55) Deng, S.; Xiao, X.; Chen, G.; Wang, L.; Wang, Y. Cd doped porous Co_3O_4 nanosheets as electrode material for high performance supercapacitor application. *Electrochim. Acta* **2016**, *196*, 316−327.
(56) Yang, Q.; Lu, Z.; Chang, Z.; Zhu, W.; Sun, J.; Liu, J.; Sun, X.; Duan, X. Hierarchical Co_3O_4 nanosheet@nanowire arrays with enhanced pseudocapacitive performance. *RSC Adv.* **2012**, *2*, 1663−1668.
(57) Hou, L.; Yuan, C.; Yang, L.; Shen, L.; Zhang, F.; Zhang, X. Urchin-like Co_3O_4 microspherical hierarchical superstructures constructed by one-dimension nanowires toward electrochemical capacitors. *RSC Adv.* **2011**, *1*, 1521−1526.
(58) Li, G.-C.; Hua, X.-N.; Liu, P.-F.; Xie, Y.-X.; Han, L. Porous Co_3O_4 microflowers prepared by thermolysis of metal-organic framework for supercapacitor. *Mater. Chem. Phys.* **2015**, *168*, 127−131.
(59) Madhu, R.; Veeramani, V.; Chen, S.-M.; Manikandan, A.; Lo, A.-Y.; Chueh, Y.-L. Honeycomb-like Porous Carbon-Cobalt Oxide Nanocomposite for High-Performance Enzymeless Glucose Sensor and Supercapacitor Applications. *ACS Appl. Mater. Interfaces* **2015**, *7*, 15812−15820.
(60) Guan, Q.; Cheng, J.; Wang, B.; Ni, W.; Gu, G.; Li, X.; Huang, L.; Yang, G.; Nie, F. Needle-like Co_3O_4 anchored on the graphene with enhanced electrochemical performance for aqueous supercapacitors. *ACS Appl. Mater. Interfaces* **2014**, *6*, 7626−7632.
(61) Wang, Y.; Lei, Y.; Li, J.; Gu, L.; Yuan, H.; Xiao, D. Synthesis of 3D-nanonet hollow structured Co_3O_4 for high capacity supercapacitor. *ACS Appl. Mater. Interfaces* **2014**, *6*, 6739−6747.
(62) Yu, M.; Zhai, T.; Lu, X.; Chen, X.; Xie, S.; Li, W.; Liang, C.; Zhao, W.; Zhang, L.; Tong, Y. Manganese dioxide nanorod arrays on carbon fabric for flexible solid-state supercapacitors. *J. Power Sources* **2013**, *239*, 64−71.
(63) Jagadale, A. D.; Kumbhar, V. S.; Dhawale, D. S.; Lokhande, C. D. Performance evaluation of symmetric supercapacitor based on cobalt hydroxide $[Co(OH)_2]$ thin film electrodes. *Electrochim. Acta* **2013**, *98*, 32−38.
(64) Hu, Q.; Gu, Z.; Zheng, X.; Zhang, X. Three-dimensional Co_3O_4@NiO hierarchical nanowire arrays for solid-state symmetric supercapacitor with enhanced electrochemical performances. *Chem. Eng. J.* **2016**, *304*, 223−231.

DOI: 10.1021/acsomega.7b00702
ACS Omega 2017, 2, 4216−4226